Sequence-Specific Rates of Interaction of Target Peptides with the Molecular Chaperones DnaK and DnaJ†

Ezra V. Pierpaoli,‡ Serge M. Gisler,‡ and Philipp Christen*

Biochemisches Institut, Universität Zürich, Winterthurerstrasse 190, CH-8057 Zürich, Switzerland

Received July 21, 1998; Revised Manuscript Received September 10, 1998

ABSTRACT: The kinetics of complex formation between nine different fluorescence-labeled peptides (7−22 amino acid residues) and DnaK (Hsp70 homologue of *Escherichia coli*) in the nucleotide-free R state and in the ATP-liganded T state were measured. R-state DnaK (1 μM) formed high-affinity complexes (K_d = 0.06−2 μM) and bound all peptides (22−50 nM) in slow one- or two-step processes with apparent rate constants for the first phase, varying only by a maximum factor of 30 (k_{obs1} = 0.003−0.084 s^{-1} at pH 7.0 and 25 °C). In contrast, the rates of complex formation between DnaK−ATP and the same peptides (K_d = 2.2−107 μM) have been found previously to vary by 4 orders of magnitude [one- or two-step processes with k_{obs1} = 0.001−7.9 s^{-1}; Gisler, S. M., Pierpaoli E. V., and Christen, P. (1998) *J. Mol. Biol. 279*, 833−840]. The slow and relatively uniform rates of peptide binding to the R state might be determined by the fraction of time during which the α-helical lid above the peptide-binding site is open. The faster and widely divergent rates of binding to the open T state might reflect sequence-specific conformational rearrangements in the peptide-binding site and perhaps of the peptide itself. The different rates of association with DnaK−ATP suggest a kinetic partitioning of target sequences in which only slowly interacting segments of polypeptides are channeled into the chaperone cycle.

The cochaperone DnaJ (Hsp40) also forms complexes with target peptides in single- to three-step processes with the apparent rate constants of the first phase varying only from 0.007 to 0.18 s^{-1}. Whether DnaJ or DnaK−ATP interact first with a target peptide might thus be determined by the individual target sequence.

Molecular chaperones of the Hsp70 type suppress improper interactions within and between unfolded polypeptide chains. They assist protein folding by stabilizing nascent polypeptides until the complete amino acid sequence is available for correct folding and by prying apart kinetically trapped folding intermediates (*1*, *2*). These effects are thought to be achieved by transient binding of exposed hydrophobic regions of the polypeptide chain that are normally buried in the interior of the folded protein (*3*) and by exerting conformational work on entangled segments (*4*). The Hsp70 chaperone system performs multiple additional functions such as facilitating translocation of polypeptides into organelles (*5*), assembling protein oligomers (*6*), disassembling clathrin-coated vesicles (*7*), participating in protein export (*8*), or targeting denatured proteins for lysosomal degradation (*9*).

DnaK, the Hsp70 homologue of *Escherichia coli*, recognizes a wide variety of heptameric hydrophobic sequences (*10*) of extended polypeptide chains (*11*, *12*). A comparison of the DnaK-binding sites of 37 proteins unraveled a common pattern: a hydrophobic core of four to five residues containing particularly Leu, but also Ile, Val, Phe, and Tyr, is flanked by regions enriched in basic residues (*13*).

The 44-kDa N-terminal ATPase domain of DnaK (*14*) and its adjacent peptide-binding unit (*10*, *15*) are structurally and functionally tightly coupled (*16*) in a K^+-dependent manner (*17*). While ADP-liganded and nucleotide-free DnaK (R state) binds peptides with high affinity and slow on and off rates, ATP-liganded DnaK (T state) displays low affinity for target peptides and fast on and off rates (*4*, *18*−*21*). The switching between the two functional states of DnaK is controlled by two cochaperones, DnaJ (41 kDa) and GrpE (22 kDa), which accelerate the rates of γ-phosphate cleavage (*20*, *22*) and facilitate ADP/ATP exchange, respectively (*22*, *23*).

Recently, we determined the kinetics of the functional cycle of the DnaK/DnaJ/GrpE molecular chaperone system using among other techniques short fluorescence-labeled target peptides to monitor their binding and release to and from DnaK (*4*, *24*). We dissected the functional cycle of the chaperone system into three kinetically defined steps: (1) DnaK−ATP binds target peptides with high on and off rates; (2) DnaJ elicits the transition of peptide−DnaK−ATP to peptide−DnaK−ADP−P_i; (3) on GrpE-induced ADP/ATP exchange, DnaK rapidly returns to its T state with concomitant forced release of the peptide (*24*). At concentrations of DnaK and the cochaperones approximating those in the cell (*25*, *26*), we identified the slow T → R transition as the rate-determining step of the system and proposed it to represent the power stroke of the chaperone cycle underlying its chaperone effects such as the sequestration of hydrophobic

† Supported in part by the Swiss National Science Foundation Grant No. 31-45940.95, the EMDO-Stiftung, Zürich, the Fonds für Medizinische Forschung der Universität Zürich, and the Ernst-Göhner Stiftung, Zürich.

* Corresponding author. Phone: +411 635 55 60. Fax: +411 635 68 05. E-mail: christen@biocfebs.unizh.ch.

‡ These authors have contributed equally to this work.

10.1021/bi981762y CCC: $15.00
Published on Web 11/04/1998

polypeptide segments and the disentangling of dead-end folding intermediates (*4*). During the T → R transition of DnaK, the bound polypeptide might be subjected to conformational work. Those previous experiments were performed with the 22-residue prepeptide of mitochondrial aspartate aminotransferase (*19*) and a shorter derivative thereof, peptide p5 (*4*), with a covalently attached fluorescent reporter group at its amino-terminal cysteine residue.

Here, we investigated with a set of nine short hydrophobic peptides (7−22 residues) to what extent the amino acid sequence of the target peptide influences the kinetics of its interaction with DnaK and DnaJ. T-state DnaK strongly discriminated between the diverse target peptides, the rates of both complex formation and dissociation varying within a range of 10^4.

MATERIALS AND METHODS

Materials. ATP−Na_2, (purity > 98%) was purchased from Fluka. *N*-[Ethyl-1,2-^{3}H]maleimide (NEM*)[1] and *N*-ethylmaleimide (NEM) were from NEN Research Products and Fluka, respectively, and 6-acryloyl-2-(dimethylamino)naphthalene (acrylodan) was from Molecular Probes, Eugene, OR. Peptides p5′ (CALLLSAARR), NR (NRLLLTG), and pσ^{32} (QRKLFFNLRKTKQ) were bought from ANAWA Wangen, Switzerland (purity > 80%). Peptides p2 (RALLQSC), p4 (CALLQSRLLS), p6 (CARSLLLSS), and $(LS)_4$ (LSLSLSLS) were synthesized by Dr. S. Klauser in our Institute with an ABI 430 A Peptide Synthesizer (Applied Biosystems) with the orthogonal Fmoc protection strategy.

Proteins. Purified DnaK was obtained as described (*19*). The nucleotide content was <0.1 mol/(mol of DnaK) (*17*). Concentration of nucleotide-free DnaK was determined photometrically with a molar absorption coefficient of ϵ_{280} = 14 500 M^{-1} cm^{-1} (*27*). DnaJ was a gift from H.-J. Schönfeld and was prepared as reported previously (*28*). The concentration of DnaJ was determined by quantitative amino acid analysis. The concentrations of both DnaK and DnaJ refer to their protomers. The preparations of DnaK and DnaJ were more than 95% pure as estimated by SDS−PAGE. Both proteins were stored at −80 °C.

Labeling of Peptides with Acrylodan. The peptides were labeled with acrylodan as described (*4*, *19*). The concentrations of the peptide stock solutions, determined by quantitative amino acid analysis, were in the range of 6−240 μM.

*Radioactive Labeling of Peptide p6 with NEM**. Possibly oxidized cysteine residues of p6 were reduced as described (*4*). For preparing a stock solution of radioactively labeled peptide, 50 μCi NEM* (49.4 Ci/mmol) in 50 μL of pentane were transferred to an ice-cooled tube containing 50 μL of 50 mM Hepes/NaOH, pH 7.0. After phase separation, the aqueous phase was freed from pentane with a stream of nitrogen, mixed with 5 μL of a 1.05 mM solution of reduced peptide p6 in 50 mM Hepes/NaOH, pH 7.0, and left for 5 min at room temperature. Nonreacted cysteine residues were blocked by adding 50 μL of 5.3 mM nonradioactive NEM in 50 mM Hepes/NaOH, pH 7.0. The reaction was allowed to proceed for 1 h at room temperature. The sample was applied to a C_8-reverse-phase HPLC column (Applied Biosystems), equilibrated with 10% acetonitrile and 0.1% trifluoroacetic acid, to separate the mono-NEM-labeled product from free and doubly conjugated peptides (alkylated at both cysteine and the α-amino group) in a linear gradient of up to 80% acetonitrile and 0.085% trifluoroacetic acid. The effluent was monitored at 215 nm. Comparison of the elution profile with that of NEM−p6 allowed identification of the NEM*-containing fractions at 27% acetonitrile. The fractions were pooled and immediately chilled on ice to impede hydrolysis of the *N*-ethylsuccinimide moiety of NEM*−p6 to the succinamic acid derivative (*29*). The volume was reduced to 10 μL in a vacuum spinner to remove volatile components such as trifluoroacetic acid and acetonitrile and then brought to 400 μL with water. As dried NEM−conjugated peptides are difficult to redissolve, the peptides were not evaporated to total dryness. Before freezing the solution in N_2 and storing it at −70 °C, samples were withdrawn for determining the radioactivity (2×10^4 cpm/μL) and the concentration of the peptide (1.9 μM). Almost 100% of the possible radioactivity was incorporated into p6.

Complex Formation between NEM−p6 and DnaK*. A mixture of NEM*−p6 (100 nM) and DnaK (2 μM) in a total volume of 700 μL was incubated at 25 °C. At the indicated times, 100-μL samples were withdrawn. DnaK was immediately separated from free peptide with Bio-Spin 6 Chromatography Columns (Bio-Rad, exclusion limit of 6 kDa). In test runs, 100 μL of a solution of either NEM*−p6 (100 nM) or DnaK (10 μM), respectively, were passed over a spin column. While ∼90% of the peptide was retained by the column, ∼80% of the DnaK was recovered.

Experimental Conditions and Buffers. All experiments were performed at 25 °C in assay buffer (25 mM Hepes/NaOH, 100 mM KCl, pH 7.0) or in assay buffer containing in addition 1 mM ATP and 5 mM $MgCl_2$. In all experiments, the samples were equilibrated for at least 5 min at 25 °C prior to measurement.

Fluorescence Measurements. (A) Slow kinetic and steady-state experiments were performed with a SPEX Fluorolog spectrofluorimeter. To measure complex formation of acrylodan-labeled peptides with DnaK, the excitation wavelength was set at 370 nm (band-pass 4.6 nm), and the emission at 500 nm (band-pass 2.25 nm) was recorded. The spectra of acrylodan-labeled peptides or of the a-peptide−DnaK complexes were scanned from 430 to 610 nm. Faster reactions in the time range of 20−100 s were initiated by adding the protein or the peptide solution with a microliter glass syringe (Hamilton, Switzerland) to the magnetically stirred peptide or protein solution. The dead time of this mixing system is approximately 3 s. The fluorescence spectra were integrated with the software provided by SPEX. Data were analyzed with Sigma Plot (Jandel Scientific).

(B) Rapid changes in fluorescence were recorded with a SF-61 stopped-flow spectrofluorimeter (HI-TECH Scientific, Salisbury) or a SX17 MV stopped-flow spectrofluorimeter (Applied Biophysics), both with a dead time of 1 ms. Reactions were initiated by mixing equal volumes (∼70 μL/syringe). The width of the entrance slit of the monochromator was set at 4−5 mm and that of the excitation slit at 5 mm. The sample was excited at 370 nm, and the emitted light passed through a GG 455 nm cutoff filter.

Reaction progress curves were fitted to either a single- or a double-exponential equation using the program Sigma Plot

[1] Abbreviations: NEM*, *N*-[Ethyl-1, 2-^{3}H]maleimide; NEM, *N*-ethylmaleimide; acrylodan, a, 6-acryloyl-2-(dimethylamino)naphthalene; pp, prepeptide of mitochondrial aspartate aminotransferase.

Table 1: Peptides Used in This Study

abbreviation[a]	sequence
a−pp	a−C**ALL**QS**RLLL**SAPRRAAATARA
p2−a	R**ALL**QSC-a
a−p4	a−C**ALL**QS**RLL**S
a−p5	a−C**LLL**SAPRR
a−p5′	a−CA**LLL**SAARR
a−p6	a−CARS**LLL**SS
a−NR	a−N**RLLL**TG
a−$(LS)_4$	a−LSLSLSLS
a−pσ^{32}	a-QR**KLFF**NLRKTKQ

[a] The letter a designates the fluorescence label acrylodan. Bold letters represent the putative binding site(s) for DnaK.

(Jandel Scientific), which provides for each evaluation the corresponding asymptotic standard deviation of the calculated parameters. In the case of stopped-flow experiments, the average of at least four measurements was analyzed with the software supplied by HI-TECH or Applied Biophysics.

Determination of Dissociation Equilibrium Constants. The dissociation equilibrium constants K_d of DnaK and DnaJ for acrylodan-labeled peptides were determined by titration of 50 or 100 nM peptide with increasing concentrations of DnaK or DnaJ in the range from 25 nM to 23 μM. K_d values were calculated by plotting the differences of areas of the fluorescence spectra from 440 to 600 nm; i.e., $\Delta A = (A_{\text{peptide−protein complex}} - A_{\text{peptide}})$(dilution factor) as a function of the total protein concentration. To attain values for K_d and ΔA_{max}, the points were fitted to the equation

$$\Delta A = \mathrm{PL}\Delta A_{max}/P_t = [\Delta A_{max}/(2P_t)][(K_d + L_t + P_t) - ((K_d + L_t + P_t)^2 - 4P_tL_t)^{0.5}]$$

where PL denotes the concentration of a-peptide−protein complexes, P_t the total protein concentration (DnaK or DnaJ), and L_t the concentration of the peptide. K_d and ΔA_{max} were chosen as parameters for the curve fitting. In some cases, the differences in fluorescence at 500 nm, $\Delta F = F_{\text{peptide−protein complex}} - F_{\text{peptide}}$, were taken for calculation. In a number of test cases, using either ΔA or ΔF gave virtually the same results.

RESULTS

Choice of Peptide Ligands. Since DnaK has been shown to bind the 22-residue prepeptide of mitochondrial aspartate aminotransferase (pp) with high affinity (*19*), short peptides corresponding to the two putative binding sites for DnaK were synthesized. Peptides p2 and p4 represent the amino-terminal binding site of pp for DnaK (Table 1). Peptide p4 was designed to test whether an elongation of the short peptide p2 would improve its affinity for DnaK. Peptides p5 and p5′ correspond to the central binding site of the prepeptide. Peptide NR was originally identified as a high-affinity ligand for DnaK in a random phage-displayed peptide library which had indicated that a positively charged residue before the central hydrophobic box favors binding (*10*). The crystal structure of the peptide-binding unit of DnaK, complexed with peptide NR, has been determined at 2.0 Å resolution (*12*). Peptide p6 was also designed on the basis of the results obtained with the phage-displayed peptides. The copolymer $(LS)_4$ provides an example of a peptide without a specific binding determinant. The constitutive

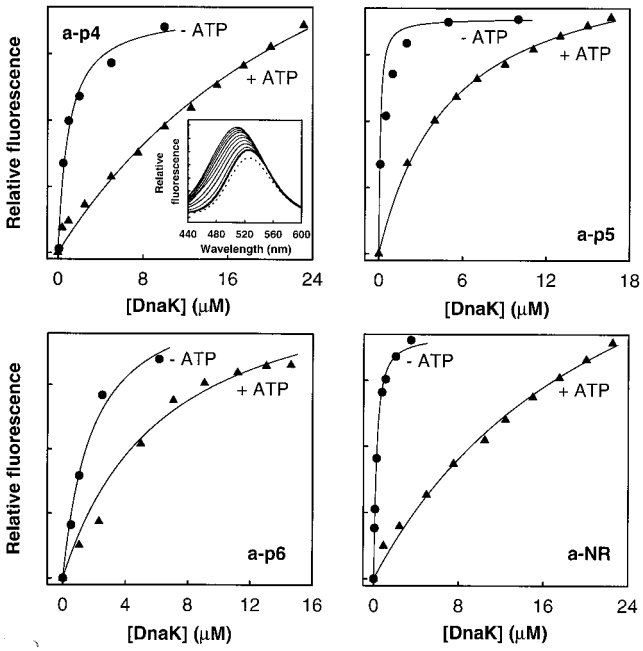

FIGURE 1: Titration of acrylodan-labeled peptides with DnaK in the absence and presence of ATP. Increasing concentrations of DnaK were added to a solution of 50 or 100 nM peptide in assay buffer alone and assay buffer with 1 mM ATP, 5 mM $MgCl_2$. On reaching the equilibrium after each addition of protein, the spectrum from 440 to 600 nm was recorded, using an excitation wavelength of 370 nm. The equilibration times were 5−30 min, depending on the peptide. As a representative example, the spectra of the titration of peptide a−p4 in the presence of ATP is shown as an inset. The differences in areas ΔA = area complex − area peptide or the differences in fluorescence at 500 nm $\Delta F = F_{\text{peptide−DnaK complex}} - F_{\text{peptide}}$ were plotted as a function of the total concentration of DnaK and fitted to an equation describing a 1:1 binding process. For details, see Materials and Methods.

binding site for DnaK in the regulatory region C of the heat shock transcription factor σ^{32} (*30*) was chosen as a natural substrate (*31*−*33*). All peptides were labeled with acrylodan either at the sulfhydryl group of their cysteine residue or at the α-amino group.

Formation of Peptide−DnaK Complexes in the Absence of ATP. Upon binding of acrylodan-labeled peptides (50 or 100 nM) to DnaK in saturating concentrations (1−23 μM), the fluorescence quantum yield of the acrylodan-labeled peptide, corresponding to the area of the fluorescence spectrum from 440 to 600 nm (see inset in Figure 1), increased, depending on the peptide, the extreme values being 1.4-fold for a−$(LS)_4$ up to 6.5-fold for a−p6. Complex formation was accompanied by a blue shift of the emission maximum of up to 30 nm (a−p6). The huge differences in the increase of fluorescence intensities and in the extent of the blue shift are to be attributed to different steric arrangements of the acrylodan label on the surface of DnaK. There is no correlation between the signal increase and the affinities of the labeled peptides for DnaK (Table 2).

In previous experiments, the apparent rate of complex formation of an acrylodan-labeled peptide with nucleotide-free DnaK proved to be only 4−5 times slower than with the ADP-liganded form of the chaperone; the K_d values of the two forms of DnaK were virtually the same (*4*). With all peptides, complex formation in the absence of ATP was slow and proved to be a two-step process in most cases (Figure 2). The apparent rate constants of the first phase

Table 2: Apparent Binding Rate Constants and Dissociation Equilibrium Constants of DnaK and Target Peptides in the Absence and Presence of ATP

peptide	k_{obs1} of first phase[a] (s^{-1})	k_{obs2} of second phase[a] (s^{-1})	first amplitude (% of total)	second amplitude (% of total)	K_d[b] (− ATP) (μM)	K_d[c] (+ ATP) (μM)
a−pp	0.013 ± 0.00005	0.002 ± 0.00005	84	16	0.063[d]	2.2[d]
p2−a	0.017 ± 0.007	0.006 ± 0.0009	78	22	1.4[d]	∼40[e]
a−p4	0.02 ± 0.002	0.009 ± 0.0003	20	80	0.95	36.1
a−p5	0.02 ± 0.0002	0.004 ± 0.00003	65	35	0.06[f]	5.1
a−p5′	0.03 ± 0.0005	0.006 ± 0.00003	34	66	0.1	41.7[g]
a−p6	0.006 ± 0.00003	0.0005 ± 0.000008	61	39	0.9	8.3
a−NR	0.003 ± 0.000007		100		0.2	23.8
a−$(LS)_4$	0.084 ± 0.004	0.02 ± 0.0005	44	56	1.8	107
a−pσ^{32}	0.008 ± 0.00006		100		1.0	100

[a] The reactions were followed with a conventional spectrofluorimeter (λ_{ex}, 370 nm; λ_{em}, 500 nm) and the time courses fitted to a single- or double-exponential function. The final concentrations were 50 nM a-peptide and 1 μM DnaK with the exception of peptide a−$(LS)_4$ and a−pσ^{32}, where 38 and 22 nM a-peptide were used. For experimental details, see legend of Figure 2 and Materials and Methods. [b] The dissociation equilibrium constants (K_d) were determined by fluorescence titration (see Materials and Methods). [c] From ref *24*. [d] From ref *19*. [e] We failed to titrate peptide p2−a because of an only insignificant increase in fluorescence intensity after addition of DnaK to the peptide. Since peptide p2−a has nearly identical binding properties to those of a−p4 (compare K_d and k_{obs} in the absence of ATP), we assumed the same K_d value for p2−a as for a−p4. [f] From ref *4*. [g] This K_d value was determined by titration of a−p5′ with DnaK (see Materials and Methods).

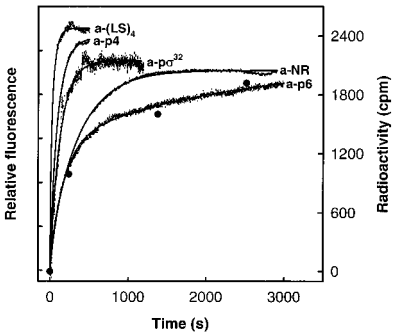

FIGURE 2: Time course of complex formation between DnaK and peptides in the absence of ATP. To ensure monomerization of DnaK, a solution of 1 μM DnaK in assay buffer was prepared and incubated for 2−10 h at room temperature. Under these conditions, DnaK can be assumed to be mainly monomeric (*44*) or in a monomer/dimer equilibrium (*45*). The reactions were started by adding the peptides, labeled with the fluorescent reporter group acrylodan, to DnaK. The changes in fluorescence at 500 nm, due to binding of labeled peptide to DnaK, were followed with a spectrofluorimeter. The final concentrations were 1 μM DnaK and 50 nM peptide, except the concentrations of a−$(LS)_4$ and a−pσ^{32} which were 38 and 22 nM, respectively. All reactions were fitted to double-exponential functions except the complex formation with peptide a−NR, which could be described by a single-exponential function. The amplitudes were normalized to be in approximately the same range. To test whether the acrylodan label was responsible for the slow binding of a−p6, the experiment was repeated with radioactively labeled peptide p6 (filled circles). For details, see Material and Methods.

varied only in a range from 0.003 to 0.084 s^{-1} (Table 2). The two-step reaction might arise from a process in which the peptide first forms an encounter complex with DnaK. In the second slower step, the peptide might become locked into a higher-affinity complex after rearrangement of DnaK, the peptide or both (*19*, *21*, *34*). A two-step mechanism might also be explained by a rearrangement of the bulky acrylodan label in the second step. To exclude this possibility, we designed a short peptide with a central tryptophan residue (SQLLLWAR). Binding of a peptide without tryptophan such as pp to DnaK did not change the intrinsic fluorescence of DnaK. Therefore, changes in tryptophan fluorescence at 340 nm upon binding of peptide SQLLLWAR to DnaK may be attributed to different environments of its tryptophan residue in the free and the DnaK-bound states. Such changes in fluorescence were indeed observed and also corresponded to a double-exponential function, indicating that the second step is not due to rearrangement of the label alone (data not shown).

To assess further the influence of the acrylodan label on the kinetics of peptide binding to DnaK, the formation of the complex between DnaK and peptide p6, marked with the small polar ^{3}H−NEM label, was followed. The time course of this reaction was quite similar to that of a−p6 (Figure 2). Apparently, the acrylodan label has only a negligible effect on the binding kinetics. The marginal influence of the acrylodan label on the equilibrium dissociation constant has also been demonstrated in a competition experiment with peptide a−p5 and the corresponding unlabeled peptide (*4*).

Dissociation Equilibrium Constants of Peptide−DnaK Complexes in the Absence of ATP. The dissociation equilibrium constants K_d between DnaK and the peptides were determined by titration of a constant concentration of peptide with increasing concentrations of DnaK (see Materials and Methods and Figure 1). Peptides with a hydrophobic core of three leucine residues (a−pp, a−p5, a−p5′, and a−NR) were found to have K_d values in the range of 60−200 nM. As an exception, a−p6 which also possesses a leucine triplet was complexed to DnaK with lower affinity (K_d = 0.9 μM; Table 2). For the second group of peptides, the K_d values ranged from 1 to 2 μM.

Binding and Release of Peptides in the Presence of ATP. On complex formation of acrylodan-labeled peptides (100 nM) with ATP-liganded DnaK (1 μM), the increase in the fluorescence quantum yield of the labeled peptide was only 20−50% of that in the absence of ATP, reflecting the lower affinity of ATP-liganded DnaK for the target peptides. Extrapolation of the titration curves in the presence of ATP (Figure 1) to saturating concentrations of DnaK still showed the maximum quantum yield of fluorescence of all peptides to be slightly lower than in the absence of ATP (data not shown). This difference together with somewhat stronger blue shifts (up to 37 nm) of the emission maxima indicates that the label is situated in different environments in the two states of DnaK.

In the presence of ATP, DnaK interacted with the different peptides in single- or double-step processes. In contrast to

Table 3: Apparent Binding Rate Constants and Dissociation Equilibrium Constants of DnaJ and Target Peptides

peptide	k_{obs1}[a] (s^{-1})	k_{obs2} (s^{-1})	k_{obs3} (s^{-1})	K_d[b] (μM)
a−p4	0.08 ± 0.003	0.002 ± 0.0002	−	nd[c]
a−p5[d]	0.1 ± 0.005	0.013 ± 0.0002	0.1 ± 0.025	37
a−NR	0.08 ± 0.007	0.0014 ± 0.0004		nd[c]
a−p6	0.007 ± 0.000015			0.3 [0.06[e]]
a−$(LS)_4$	0.18 ± 0.05			nd[c]
a−pσ^{32}	0.06 ± 0.0004			92 ± 60

[a] A stopped-flow spectrofluorimeter was used for experiments conducted with peptides a−$(LS)_4$, a−pσ^{32}, and a−p6. The reactions with peptides a−p4 and a−NR were carried out with a conventional spectrofluorimeter equipped with a syringe system (see Materials and Methods). Final concentrations were as follows: a−p4, a−NR, a−pσ^{32}, 100 nM; DnaJ, 1 μM, and 2 μM in the experiments with a−p6 and a−$(LS)_4$. Experimental conditions are outlined in the legend of Figure 3. [b] Constants were obtained by fluorescence titration as described under Materials and Methods. [c] Not determined. [d] From ref *4*. [e] K_d value calculated from k_{-1} and k_{obs}.

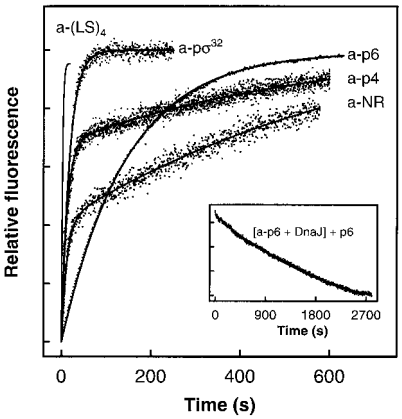

FIGURE 3: Reaction traces of the interaction of the cochaperone DnaJ with peptides. The reactions were started either by mixing equal volumes of a solution containing peptide (a−p6, a−$(LS)_4$, and a−pσ^{32}) and DnaJ with a stopped-flow appliance, or by injecting DnaJ with the syringe system (see Materials and Methods) to the continuously stirred peptide solution (a−p4 and a−NR). The excitation wavelength was 370 nm and the emitted light was either, in the case of stopped-flow measurements, passed through a GG 455 cutoff filter or detected at 500 nm in the spectrofluorimetric measurements. All experiments were performed in assay buffer. Final concentrations were as follows: a-peptide, 100 nM; DnaJ, 1 μM for (a−p4 + DnaJ), (a−NR + DnaJ) and (a−pσ^{32} + DnaJ) or DnaJ, 2 μM for (a−p6 + DnaJ) and (a−$(LS)_4$ + DnaJ). Normalized data were fitted to a single- or a double-exponential equation. Inset: Displacement of a−p6 from preformed DnaJ−a−p6 complex by excess unlabeled peptide p6. Prior to the addition of the competitor p6, complex formation of DnaJ and a−p6 was allowed to reach equilibrium. The final concentrations were 200 nM a−p6, 200 μM p6, and 3 μM DnaJ.

the similar apparent rates for the formation of a−peptide−DnaK complexes in the absence of ATP, the rates in the presence of ATP, as reported previously (*24*), varied widely over 4 orders of magnitude from 0.001 to 7.9 s^{-1} (Table 4 in Discussion).

In conformity with previously published results (*4*, *19*), the affinities for peptides to DnaK were reduced 5- to 100-fold in the presence of ATP with K_d values from 2.2 μM to more than 100 μM (Table 2). Peptides forming high-affinity complexes in the absence of ATP, e.g. a−p5, a−pp, and a−NR, bound also with relatively high affinity in the presence of ATP.

Formation of Peptide−DnaJ Complexes. Complex formation of acrylodan-labeled peptides with DnaJ occurred in up to three phases depending on the peptide (Figure 3). The apparent rate constants of the first phase were in the range of 0.007 s^{-1} (a−p6) up to 0.18 s^{-1} (a−$(LS)_4$) (Table 3). The peptide−DnaJ complexes were slightly less tight than those with DnaK in the presence of ATP. Upon addition of 100 nM a−p6 to 1 μM DnaJ, the peptide fluorescence augmented 3.7-fold, which was much higher than the maximally 1.4-fold increase observed with other peptides. The signal was even higher than that for a−p6−DnaK which is the highest increase in fluorescence (2.2-fold) observed with any a-peptide binding to DnaK. To confirm the strong binding of a−p6 ($K_d \sim 0.3$ μM; Table 3), we preformed the complex of a−p6 with DnaJ and measured the displacement of a−p6 by adding excess unlabeled p6 (Figure 3, inset). The observed time course followed a single-step reaction with an extremely slow dissociation rate constant of 0.0004 s^{-1}. From k_{obs1} and k_{-1}, the on rate constant k_{+1} was calculated to be 6600 M^{-1} s^{-1}. The K_d value of a−p6 for DnaJ (60 nM), determined from the association and dissociation rates, proved to be in a range similar to that of the K_d value determined by titration (300 nM). Thus, a−p6 seems to possess at least a 25-fold higher affinity to DnaJ than for DnaK−ATP (cf. Table 2). Moreover, a−p6 associates with DnaK−ATP 150 times more slowly than with DnaJ at identical dissociation rates. From K_d and k_{obs} for the complex formation between DnaJ and a−pσ^{32} (Table 3), k_{+1} and k_{-1} were calculated to be 650 M^{-1} s^{-1} and 0.06 s^{-1}, respectively.

DISCUSSION

Formation of Peptide−DnaK Complexes in the Absence of ATP. Considering the very slow overall rates of the interaction of target peptides with the R state of DnaK (Table 2), binding and release of target peptides to this state of the chaperone can be assumed to be of no functional relevance in vivo. Determination of the crystal structure of the peptide-binding domain of DnaK (residues 384−609) has revealed a peptide-binding channel and a movable lid on the top of it that encapsulates the substrate in the channel (*12*). In the ADP state of DnaK, the lid is supposed to be predominantly closed. Binding of ATP is thought to result in a shift of the conformational equilibrium toward the open conformation of the lid and thus in better accessibility of the peptide-binding channel. One possibility for the peptide substrate to enter the binding channel of DnaK−ADP would be by threading its way in. This mechanism, however, seems to be rather improbable with a peptide (*12*) and virtually impossible with a substrate protein. Presumably, the lid opens and closes also in the ADP state of DnaK, albeit for a much shorter period of time than in the ATP state. According to this notion, the velocity of binding of peptides to DnaK−ADP would be mainly controlled by the position

Table 4: Association and Dissociation Rate Constants for the First Step of the Peptide−DnaK Complex Formation in the Presence of ATP[a]

peptide	k_{obs1} (s^{-1})	k_{+1} (M^{-1} s^{-1})	k_{-1} (s^{-1})
a−pp	2.3	450 000	1.8
p2−a[b]	0.2	5 350	0.2
a−p4	7.9	55 000	7.2
a−p5	6.8	1 115 000	5.7
a−p5′ [b]	1.6	37 500	1.6
a−p6	0.001	44	0.0004
a−NR	5.9	104 000	4.5
a−$(LS)_4$	0.04	96	0.04
a−pσ^{32}	0.017	390	0.024

[a] All values are from ref *24*, unless indicated otherwise. In the case of biphasic reactions, the values correspond to the first phase, i.e., formation of the encounter complex, and were determined by measuring the apparent rate constants of peptide−DnaK complex formation at a constant concentration of peptide and varying concentrations of DnaK (*24*). [b] From the K_d values for the peptide−DnaK complex formations (Table 2) in the presence of ATP and the apparent rate constants k_{obs1}, k_{on}, and k_{off} were calculated for the monophasic reactions according to ref *24*. The conditions were as follows: a−p5′, 50 nM; p2−a, 100 nM; DnaK, 1 μM; pH 7.0; 25 °C.

of the equilibrium between the open and closed states of the α-helical lid and would be largely independent of the nature of the peptide. Indeed, the apparent rate constants of complex formation of different peptides with R-state DnaK vary only by a maximal factor of 30 (Table 2). In contrast, the rates of complex formation with T-state DnaK range within 4 orders of magnitude (Table 4).

Dissociation Equilibrium Constants of Peptide−DnaK Complexes in the Absence of ATP. A first group of peptides containing a hydrophobic core of three Leu residues (a−pp, a−p5, a−p5′, and a−NR; Table 1) were bound with very high affinity corresponding to K_d values in the range of 60−200 nM (Table 2). The crystal structure of the substrate-binding domain of DnaK complexed with peptide NR shows that the main interactions between the peptide and the chaperone are seven main-chain hydrogen bonds and numerous van der Waals contacts from its side chains (*12*). A crucial anchoring point is a deep hydrophobic pocket in the peptide-binding channel, referred to as "position 0", into which the central Leu, Leu4 of peptide NR (see Table 1), is accommodated. Leu3 and Leu5 at subsites −1 and +1 of DnaK, respectively, contribute also to hydrophobic interactions, the effect of Leu5 being the least. The present data confirm that a box of three consecutive Leu residues is important for high-affinity binding to DnaK. Peptide a−p6 seems to constitute a special case since it contains a leucine triplet but binds with a K_d value of 0.9 μM. Presumably, the increased distance between its arginine residue and the leucine triplet due to an inserted serine residue (Table 1) interferes with high-affinity binding. Positively charged side chains flanking the leucine triplet are supposed to interact with the negatively charged surface surrounding the peptide-binding channel of DnaK (*12*).

In the second group of peptides, the K_d values were between 1 and 2 μM. The binding sites of these ligands (Table 1) comprised an LL doublet (e.g. p2−a and a−p4), an LFF binding motif (a−pσ^{32}), or an alternating sequence of Leu and Ser (a−$(LS)_4$). It seems that omission of one Leu residue from the LLL triplet brings about a 10- to 20-fold reduction in affinity of the peptide for DnaK. Phenylalanine may replace leucine without impairing the binding (a−pσ^{32}). Generally, our results agree with previous reports on the substrate preference of DnaK (*10*, *13*). The virtually identical affinity of DnaK for a−p5 and a−pp strongly suggests that the main binding site of the prepeptide for DnaK lies in its middle part (Table 1).

Binding and Release of Peptides in the Presence of ATP. In the T state of DnaK, the lid of the peptide binding site has been proposed to be open, allowing rapid diffusion of the peptide into the binding crevice (*12*). On and off rates range from 44 M^{-1} s^{-1} (a−p6) up to 1 115 000 M^{-1} s^{-1} (a−p5) and from 0.0004 s^{-1} (a−p6) up to 7.2 s^{-1} (a−p4), respectively (Table 4). Highest on and off rates were obtained with peptides a−pp, a−p4, a−p5, and a−p5′, all possessing a hydrophobic core composed of two or three Leu residues. Strikingly, if a positively charged residue preceded the hydrophobic box (p2−a, a−p6, a−pσ^{32} in Table 1), both the on and the off rates were significantly reduced (Table 4). A positively charged residue preceding the hydrophobic box seems to have a rate-decreasing effect.

The marked differences in the kinetics of binding of different peptides (k_{on}) imply that structural features of the peptide itself, such as sequence and length, determine the time required for positioning the peptide into the cleft. A higher rate of peptide-binding correlates with a higher rate of peptide release (Table 4). Consequently, the K_d values vary in a relatively narrow range (Table 2). Apparently, the structure of the DnaK−peptide complex is similar in all cases tested.

Formation of Peptide−DnaJ Complexes. The cochaperone DnaJ has been found to bind to various native proteins such as the RepA replication initiator protein (*35*, *36*), the σ^{32} transcription factor (*32*, *36*), and several denatured proteins, e.g. molten-globule-like folded rhodanese (*37*) or unfolded luciferase (*38*). Complexes of DnaJ were also found with peptides, for example with the amino-terminal 17 amino acid residues of native bovine rhodanese (*39*) and variants of a−p5′ (Table 1) composed of D-amino acids (*40*). By binding to a polypeptide, a DnaJ molecule may become located close to a molecule of DnaK−ATP bound to the same target. The spatial proximity of polypeptide-bound DnaJ and DnaK will facilitate the stimulation of γ-phosphate cleavage of DnaK-bound ATP by DnaJ (*20*, *38*). Since it is known from cross-linking experiments (*41*) that DnaJ is able to interact with nascent polypeptides on prokaryotic ribosomes, short peptides without secondary structure seem to constitute adequate substrates for DnaJ. Our results agree with the observation that DnaJ binds short extended peptides (*39*). DnaJ was proposed to be the first chaperone to interact with a nascent chain or an unfolded polypeptide, thereby targeting them for DnaK (*38*, *41*). However, the rates of complex formation as reported in this study suggest that the sequence of the polypeptide determines whether DnaJ or DnaK−ATP is the first binding partner. Since the apparent rates for the first phase of complex formation between DnaJ and peptides lie in a relatively narrow range and are slow (k_{obs1} = 0.007−0.18 s^{-1}) and the corresponding rates k_{obs1} for complex formation with DnaK−ATP vary over a much broader range from 0.001 to 7.9 s^{-1} (Table 4), it seems that the velocity of binding to DnaK−ATP decides whether DnaJ or DnaK−ATP binds the target peptide first. Values of $k_{obs1} > 0.2$ s^{-1} for the interaction with DnaK−ATP are expected to result

Scheme 1

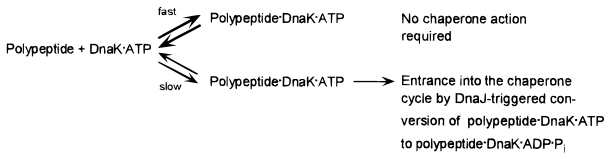

in binding to DnaK−ATP rather than to DnaJ. This estimate does not take into consideration that the intracellular concentration of DnaJ very likely is below 1 μM (*25*, *26*) as used in these measurements (Table 3), resulting in even slower rates of complex formation.

CONCLUSIONS

The rates of peptide binding and release in the case of R-state DnaK proved to vary in a limited range for the different peptides tested. Apparently, the open/closed equilibrium of the lid of the peptide-binding domain largely determines the rate of interaction. In contrast, the tested peptides possessed widely distributed on and off rates with the T state of DnaK, albeit they were of similar length and sequence. Conceivably, the differences reflect conformational rearrangements of the peptide-binding site and perhaps the peptide itself that largely depend on its sequence. The peptides might differ in the position of the equilibrium between unstructured and secondary-structured forms, between monomer, dimer, and oligomers or, in the case of proline-containing peptides, cis and trans isomers. However, circular dichroism measurements of several peptides (pp, NEM-coupled p4 and p6, ala−p5, p5 with amino-terminal alanine instead of cysteine, and NR) in the presence of the α-helix-inducing agent trifluoroethanol showed no correlation between the α-helix propensity of a particular peptide and the rate of its binding or its release (data not shown).

The vastly diverging rates of interaction of different peptides with DnaK−ATP (Table 4) might reflect the existence of a kinetic partitioning mechanism that channels slowly interacting segments of polypeptide chains into the chaperone cycle (Scheme 1). Peptides pp, p4, p5, p5′, and NR associate very quickly with DnaK−ATP and presumably are already in an extended conformation, fitting optimally into the binding cavity of DnaK. These substrates might not require any disentangling in the DnaK chaperone cycle and are instantly released without hydrolysis of ATP. In contrast, binding and release to and from DnaK−ATP is much slower for other peptides such as p2, p6, $(LS)_4$, or pσ^{32}. They might adopt alternative conformations and might have to be subjected to conformational work during the DnaJ-triggered T → R conversion in order to be positioned in extended form into the peptide-binding channel of DnaK. The DnaJ-triggered conversion of peptide−DnaK−ATP to peptide−DnaK−ADP−P_i takes place with apparent rate constants $k_{obs} = 0.04-0.14$ s^{-1} at 1 μM DnaK, 1 μM DnaJ, and 25 °C (*4*, *42*). In the case of the slowly released peptides, the time of residence of the peptide in the binding site is prolonged as compared to fast interacting peptides with similar K_d values. The probability of successful interaction of the peptide−DnaK complex with DnaJ is thus strongly increased. The kinetic partitioning mechanism would channel only those polypeptide segments into the chaperone cycle that have to be disentangled or stretched for productive protein folding. Fast binding and released peptides dissociate from DnaK−ATP prior to the stimulation of γ-phosphate cleavage by DnaJ.

A similar mechanism pertains to the GroEL-chaperone of *E. coli* (*43*). Fast folding proteins are ejected as native structures from GroEL before ATP hydrolysis, while slowly folding proteins enter the chaperone cycles of annealing and folding after initial ATP hydrolysis.

ACKNOWLEDGMENT

We are grateful to Heinz Gehring and Hans-Joachim Schönfeld for helpful discussions, and we thank Peter Hunziker, Ragna Sack, and Peter Gehrig for quantitative amino acid analyses as well as for mass spectra.

REFERENCES

1. Hartl, F.-U. (1996) *Nature 381*, 571.
2. Bukau, B., Hesterkamp, T., and Luirink, J. (1996) *Trends Cell Biol. 6*, 480−486.
3. Flynn, G. C., Pohl, J., Flocco, M. T., and Rothman, J. E. (1991) *Nature 353*, 726−730.
4. Pierpaoli, E. V., Sandmeier, E., Baici, A., Schönfeld, H.-J., Gisler, S., and Christen, P. (1997) *J. Mol. Biol. 269*, 757−768.
5. Schatz, G., and Dobberstein, B. (1996) *Science 271*, 1519−1526.
6. Frydman, J., Nimmesgern, E., Ohtsuka, K., and Hartl, F.-U. (1994) *Nature 370*, 111−117.
7. Gao, B., Biosca, J., Craig, E. A., Greene, L. E., and Eisenberg, E. (1991) *J. Biol. Chem. 266*, 19565−19571.
8. Wild, J., Altman, E., Yura, T., and Gross, C. (1992) *Genes Dev. 6*, 1165−1172.
9. Hayes, S. A., and Dice, J. F. (1996) *J. Cell Biol. 132*, 255−258.
10. Gragerov, A., Zeng, L., Zhao, X., Burkholder, W., and Gottesman, M. E. (1994) *J. Mol. Biol. 235*, 848−854.
11. Landry, S. J., Jordan, R., McMacken, R., and Gierasch, L. M. (1992) *Nature 355*, 455−457.
12. Zhu, X., Zhao, X., Burkholder, W. F., Gragerov, A., Ogata, C. M., Gottesman, M. E., and Hendrickson, W. A. (1996) *Science 272*, 1606−1614.
13. Rüdiger, S., Germeroth, L., Schneider-Mergener, J., and Bukau, B. (1997) *EMBO J. 16*, 1501−1507.
14. Chappell, T. G., Konforti, B. B., Schmid, S. L., and Rothman, J. E. (1987) *J. Biol. Chem. 262*, 746−751.
15. Wang, T.-F., Chang, J., and Wang, C. (1993) *J. Biol. Chem. 268*, 26049−26051.
16. Buchberger, A., Theyssen, H., Schröder, H., McCarty, J. S., Virgallita, G., Milkereit, P., Reinstein, J., and Bukau, B. (1995) *J. Biol. Chem. 270*, 16903−16910.
17. Feifel, B., Sandmeier, E., Schönfeld, H.-J., and Christen, P. (1996) *Eur. J. Biochem. 237*, 318−321.
18. Palleros, D. R., Reid, K. L., Shi, L., Welch, W. J., and Fink, A. L. (1993) *Nature 365*, 664−666.
19. Schmid, D., Baici, A., Gehring, H., and Christen, P. (1994) *Science 263*, 971−973.
20. McCarty, J. S., Buchberger, A., Reinstein, J., and Bukau, B. (1995) *J. Mol. Biol. 249*, 126−137.
21. Takeda, S., and McKay, D. B. (1996) *Biochemistry 35*, 4636−4644.
22. Liberek, K., Marszalek, J., Ang, D., Georgopoulos, C., and Zylicz, M. (1991) *Proc. Natl. Acad. Sci. U.S.A. 88*, 2874−2878.
23. Packschies, L., Theyssen, H., Buchberger, A., Bukau, B., Goody, R. S., and Reinstein, J. (1997) *Biochemistry 36*, 3417−3422.
24. Gisler, S. M., Pierpaoli, E. V., and Christen, P. (1998) *J. Mol. Biol. 279*, 833−840.
25. Bardwell, J. C. A., Tilly, K., Craig, E., King, J., Zylicz, M., and Georgopoulos, C. (1986) *J. Biol. Chem. 261*, 1782−1785.

26. Goodsell, D. S. (1991) *Trends Biochem. Sci. 16*, 203−206.
27. Helleburst, H., Uhlén, M., and Enfors, S. O. (1990) *J. Bacteriol. 172*, 5030−5034.
28. Schönfeld, H.-J., Schmidt, D., and Zulauf, M. (1995) *Prog. Colloid Polym. Sci. 99*, 7−10.
29. Gehring, H., and Christen, P. (1980) *Anal. Biochem. 107*, 358−361.
30. McCarty, J. S., Rüdiger, S., Schönfeld, H.-J., Schneider-Mergener, J., Nakahigashi, K., Yura, T., and Bukau, B. (1996) *J. Mol. Biol. 256*, 829−837.
31. Gamer, J., Bujard, H., and Bukau, B. (1992) *Cell 69*, 833−842.
32. Gamer, J., Multhaup, G., Tomoyasu, T., McCarty, J. S., Rüdiger, S., Schönfeld, H.-J., Schirra, C., Bujard, H., and Bukau, B. (1996) *EMBO J. 15*, 607−617.
33. Liberek, K., Wall, D., and Georgopoulos, C. (1995) *Proc. Natl. Acad. Sci. U.S.A. 92*, 6224−6228.
34. Hiromi, K. (1979) *Kinetics of Fast Enzyme Reactions*, Halsted Press, New York.
35. Wickner, S., Hoskins, J., and McKenney, K. (1991) *Proc. Natl. Acad. Sci. U.S.A. 88*, 7903−7907.
36. Wawrzynów, A., and Zylicz, M. (1995) *J. Biol. Chem. 270*, 19300−19306.
37. Langer, T., Lu, C., Echols, H., Flanagan, J., Hayer, M. K., and Hartl, F.-U. (1992) *Nature 356*, 683−689.
38. Szabo, A., Langer, T., Schröder, H., Flanagan, J., Bukau, B., and Hartl, F.-U. (1994) *Proc. Natl. Acad. Sci. U.S.A. 91*, 10345−10349.
39. Kudlicki, W., Odom, O. W., Kramer, G., and Hardesty, B. (1996) *J. Biol. Chem. 271*, 31160−31165.
40. Feifel, B., Schönfeld, H.-J., and Christen, P. (1998) *J. Biol. Chem. 273*, 11999−12002.
41. Hendrick, J. P., Langer, T., Davis, T. A., Hartl, F.-U., and Wiedmann, M. (1993) *Proc. Natl. Acad. Sci. U.S.A. 90*, 10216−10220.
42. Gisler, S. M. (1997) Diploma thesis, University of Zurich, Zurich, Switzerland.
43. Corrales, F. J., and Fersht, A. R. (1996) *Proc. Natl. Acad. Sci. U.S.A. 93*, 4509−4512.
44. Palleros, D. R., Reid, K. L., Shi, L., and Fink, A. L. (1993) *FEBS Lett. 336*, 124−128.
45. Schönfeld, H.-J., Schmidt, D., Schröder, H., and Bukau, B. (1995) *J. Biol. Chem. 270*, 2183-2189.

BI981762Y